COMPEL - The international journal for computation and mathematics in electrical and electronic engineering

Effective reluctivity of an insulated magnetic spherical particle excited by an axisymmetric polar magnetic field

Joonas Vesa
Graduate School of Information Science and Technology, Hokkaido University, Sapporo, Japan, and Faculty of Engineering, Graduate School of Engineering, Kyoto University, Kyoto, Japan

Shingo Hiruma
Graduate School of Information Science and Technology, Hokkaido University, Sapporo, Japan

Timo Tarhasaari
Electrical Engineering Unit, Tampere University, Tampere, Finland, and

Tetsuji Matsuo
Faculty of Engineering, Graduate School of Engineering, Kyoto University, Kyoto, Japan

Received 21 November 2025
Revised 8 April 2026
Accepted 14 May 2026

Abstract

Purpose – The purpose of this study is to provide a formula for the homogenized reluctivity of an electrically insulated spherical conductive magnetic particle. The insulated particle is excited by azimuthally symmetric boundary conditions for the magnetic field in the polar direction. Otherwise, the boundary conditions are arbitrary.

Design/methodology/approach – A magnetodynamic formulation of Maxwell's equations is considered inside the particle. An electrostatic formulation is considered inside the insulation. The homogenized reluctivity is derived using mathematical methods based on analytical solutions of the formulations. The leading principle in the derivation of the homogenized reluctivity is energy consistency.

Findings – The most important finding is the formula for the homogenized reluctivity. Furthermore, considering an orthogonal decomposition of the magnetic flux density in terms of spherical harmonics, it turns out that homogenization only distinguishes the first mode of the flux density, regardless of which modes are excited by the boundary conditions. This result is somewhat expected, but it forces us to lump the energy exchange of the higher modes into the homogenized magnetic field strength. The treatment also exposes some of the mathematical structures required for homogenization.

Funding: This work was funded by the foundation of Ulla Tuominen through the Foundations' Post Doc Pool. This project has received funding from the European Research Council (ERC) under the European Union's Horizon 2020 research and innovation programme (grant agreement No 848590). The Academy of Finland is also acknowledged for financial support (grant No 346440).

COMPEL - The international journal for computation and mathematics in electrical and electronic engineering
Emerald Publishing Limited
0332-1649
DOI 10.1108/COMPEL-11-2025-0574

Originality/value – The formula for the homogenized reluctivity is novel. It admits arbitrary but rotationally symmetric boundary conditions for the magnetic field strength at the outer boundary of the insulation in the polar direction. Industrial applications of the developed methods include powder-like materials such as soft magnetic composites. New perspectives on homogenization are provided.

Keywords Homogenization, Magnetic sphere, Soft magnetic composite, Spherical harmonics

Paper type Research paper

1. Introduction

In this study, an electrically insulated conductive magnetic particle is homogenized. Homogenization refers to treating the material inside the domain as homogeneous and determining an appropriate material model for it. The motivation for such a study partly arises from the homogenization of soft magnetic composite (SMC) materials. More importantly, the theoretical aspects provide strong motivation. It turns out that by using orthogonal decompositions for the fields, a homogenized reluctivity for an insulated particle can be derived analytically for a variety of boundary conditions. This additional freedom in the choice of boundary conditions makes it possible to study how different boundary conditions and insulation types affect losses and other system dynamics in a more detailed manner. Since the methodology is analytical, it does not suffer from numerical instabilities such as air-gap meshing issues. Furthermore, the analytical treatment reveals certain mathematical structures that are essential for performing such homogenization.

SMC materials consist of compressed, insulated ferromagnetic powders (Shokrollahi and Janghorban 2007). Modeling the behavior of SMC materials is motivated by their commercial applications, such as inductors and transformers, which can operate at higher frequencies than laminated steels owing to their finer resistive structures. Prof. Igarashi's group explored a semi-analytical method for modeling SMC materials (Sato and Igarashi, 2016, Sato *et al.*, 2015, Sato and Igarashi, 2017). It is based on the homogenized permeability of a single spherical particle, which is materially homogeneous. The study assumes a specific form of boundary conditions for the magnetic field. These conditions ensure uniform magnetic excitation and prevent any currents from flowing through the boundary. It is questionable if the assumption of uniform magnetic excitation holds for the particles in SMC materials. If a particle is surrounded by other particles, questions arise if other magnetic modes are excited in the particle than just the uniform mode. Furthermore, it would be beneficial for practical applications to also take into account the insulation surrounding the particle.

In more recent studies, the same form of homogenized permeability has also been applied to the modeling of randomized materials (Sato *et al.*, 2024). These studies help to understand the logic behind homogenization; the material model is redefined such that the particle-scale geometry can be replaced by a homogeneous material. Homogenized material models are often found by equating energy-related quantities in a unit cell (Ito and Igarashi 2013; Ren *et al.*, 2016; Corcolle *et al.*, 2021; Maruo and Igarashi, 2019; H. Sato and Igarashi, 2021).

Whereas some modeling approaches emphasize homogenization, others emphasize multiscale. Corcolle *et al.* (Corcolle et al., 2021) and Bottauscio *et al.* (Oriano Bottauscio *et al.*, 2006; Bottauscio *et al.*, 2009; Bordianu *et al.*, 2012) have studied and applied multiscale methods. Some methods, such as those presented in Bottauscio's papers, rely on mathematical multiscale methods. Others build on the idea that Maxwell's equations should remain invariant under homogenization, and that the information exchanged between spatial scales should consist solely of field quantities. Consequently, the computational subproblems

can be interpreted as homogenized material models. Corcolle's work is based on this latter line of reasoning.

Kameari investigated magnetic modes in spherical regions in Japanese literature (Kameari 2015, Advanced Electromagnetic Field Analysis for Effective Design, 2016). He established relationships between each pair of magnetic *h*-modes and *b*-modes. Furthermore, he identified Cauer networks that represent these relationships.

In this study, a homogenized reluctivity for an insulated particle is derived. It admits arbitrary but azimuthally symmetric boundary conditions for the *h*-field in the polar direction. The homogenized reluctivity is energy-consistent, meaning that the point-wise relation between the homogenized *h*- and *b*-field carries the same power losses as what is transferred through the boundary of the particle/insulation system. Orthogonal spherical magnetic modes are exploited, and connections between the modes, their boundary conditions and homogenized quantities are provided.

The remainder of this paper is organized as follows. The treatment for a particle is provided in Section 2. The treatment is extended to include the region of insulation around the particle in Section 3. Numerical examples are provided in Section 4, and the conclusions are presented in Section 5.

2. Particle

We use a spherical coordinate system, as shown in Figure 1(a). The spherical coordinates (r, θ, ϕ) are transformed into Cartesian coordinates (x, y, z) as follows:

$$\begin{cases} x = r \sin\theta \cos\phi, \\ y = r \sin\theta \sin\phi, \\ z = r \cos\theta. \end{cases} \tag{1}$$

We denote r as the radial coordinate, θ as the polar coordinate and ϕ as the azimuthal coordinate. The corresponding coordinate co-frames are denoted as $\mathrm{d}r$, $\mathrm{d}\theta$ and $\mathrm{d}\phi$. They are differential 1-forms (Lindell 2004).

We first homogenize one spherical magnetic particle of radius R_{prt}, centered around the origin of the coordinate system, as depicted in Figure 1(a). The particle is surrounded by insulation, but we do not yet include the insulating region $R_{\mathrm{prt}} < r < R_{\mathrm{ins}}$ in the model. In this

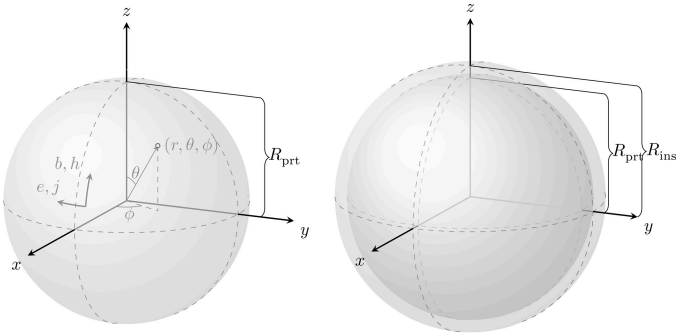

Figure 1. Spherical particle and the directions of the fields. (a) Particle, (b) Particle/insulation-system

section, we consider the insulated nature of the particle by assuming such a representation of the electric field inside the particle that admits no current density through the boundary. The results of this section are used in Section 3, where the insulation, visualized in Figure 1(b), is also fully considered.

2.1 Field solutions

We assume that our magnetic excitations are symmetric with respect to rotations around the Cartesian z-axis. The fields expressed in spherical coordinates do not depend on the azimuthal coordinate ϕ. We express the fields as differential forms (Lindell, 2004). This provides greater clarity in the treatment of spherical coordinates and later reveals a mathematical structure essential for homogenization.

The physics inside the particle is described by the magnetic field strength h, current density j, electric field strength e and magnetic flux density b. The fields are modeled by the equations:

$$\mathrm{d}h = j, \tag{2}$$

$$\mathrm{d}e = -i\omega b, \tag{3}$$

$$\mathrm{d}b = 0, \tag{4}$$

$$b = \star\mu h, \tag{5}$$

$$j = \star\sigma e, \tag{6}$$

where i is the imaginary unit, ω is the angular frequency and μ and σ denote the permeability and conductivity of the particle, respectively. The material parameters are assumed to be constant within the particle. Furthermore, d is the exterior derivative, and the operator $\star$ is the Hodge star, defined by the identity $\alpha\wedge\star\beta = <\alpha, \beta>\eta$ for all differential forms α and β of equal degree, where η is the volume form and $<\cdot, \cdot>$ is the usual inner product of forms. The Hodge star has a unique inverse. In three dimensions, one has $\star^{-1} = \star$.

Magnetodynamic equation in terms of the electric field e in the frequency domain is:

$$\star^{-1}\mathrm{d}\star^{-1}\mathrm{d}e = \underbrace{(-i\omega\mu\sigma)}_{k^2} e, \tag{7}$$

For a circumferential electric field $e = e_\phi \mathrm{d}\phi$, equation (7) has the solution:

$$e = \sum_{n=1}^{\infty} -\alpha_n r j_n(kr) Y_n^1(\theta, \phi) \sin\theta \mathrm{d}\phi, \tag{8}$$

where α_n are coefficients to be determined later by the boundary conditions, j_n is the nth spherical Bessel function and Y_n^1 are scalar spherical harmonic functions (see for example Abramowitz and Stegun, 1965). We denote a (closed) ball around the origin with radius R as B_R. We define the inner product $<\cdot, \cdot>_{\partial B_R}$ and normalize the spherical harmonics as:

$$\langle Y_n^1 \mathrm{d}\theta,\, Y_m^1 \mathrm{d}\theta \rangle_{\partial B_R} := \int_{\partial B_R} Y_n^1(\theta,\phi) Y_m^{1\,*}(\theta,\phi) \sin\theta \mathrm{d}\theta \wedge \mathrm{d}\phi = \delta_{nm}, \tag{9}$$

where * denotes the complex conjugation and the symbol $\delta_{nm} = 1$, if $n = m$, and $\delta_{nm} = 0$ otherwise. The inner product on the surface ∂B_R is independent of radius R, because the spherical harmonics and $\sin\theta$ do not depend on the radial coordinate and $\mathrm{d}\theta$ and $\mathrm{d}\phi$ are coordinate co-frames.

Defining a magnetic vector potential as $a = -\frac{1}{i\omega} e$, we have:

$$a = \sum_{n=1}^{\infty} \frac{\alpha_n}{i\omega} r j_n(kr) Y_n^1(\theta,\phi) \sin\theta \mathrm{d}\phi, \tag{10}$$

from which we calculate:

$$b = \sum_{n=1}^{\infty} \frac{\alpha_n}{i\omega} \left[-\frac{\partial}{\partial r}\left(r j_n(kr)\right) Y_n^1(\theta,\phi) \sin\theta \mathrm{d}\phi \wedge \mathrm{d}r \underbrace{+ r j_n(kr) \frac{\partial}{\partial\theta}\left(Y_n^1(\theta,\phi)\sin\theta\right)}_{\text{normal component}} \mathrm{d}\theta \wedge \mathrm{d}\phi \right], \tag{11}$$

$$h = \sum_{n=1}^{\infty} \frac{\alpha_n}{i\omega\mu} \left[\underbrace{-\left(j_n(kr) + kr j_n'(kr)\right) Y_n^1(\theta,\phi)}_{\text{tangential component}} \mathrm{d}\theta + j_n(kr) \frac{\partial}{\partial\theta}\left(Y_n^1(\theta,\phi)\sin\theta\right) \frac{1}{r\sin\theta} \mathrm{d}r \right], \tag{12}$$

in which j_n' denotes the derivative of j_n with respect to the inner function.

2.2 Homogenization of the magnetic flux density

It is well known that the b-field is homogenized by spatial averaging (Bossavit, 1995; Gyselinck, Vandevelde *et al.*, 1999; Gyselinck, Sabariego, and Dular 2006). This step involves a decision. The b-field can indeed be averaged spatially, but as a 2-form it must be averaged against a vector frame that is considered to be spatially constant. Because we are dealing with homogenization, we are interested in the Cartesian components of the b-field. We define the homogenized flux density $b_{\mathrm{prt}}^{\mathrm{eff}}$ as the spatial average of the Cartesian z-component of the b-field over the volume of the particle. The spatial average can be calculated by considering the magnetic potential a on the boundary. First, we calculate the magnetic flux Φ_θ through a surface S_z which is the intersection of the particle with a plane whose z-coordinate is constant. The surface is oriented counterclockwise around the z-axis. Its boundary is the circle $\phi \to (R_{\mathrm{prt}}, \theta, \phi)$ for a fixed θ and R_{prt}. We have:

$$\Phi_\theta = \int_{S_z} \mathrm{d}a = \int_{\partial S_z} a = 2\pi \sum_{n=1}^{\infty} \frac{\alpha_n}{i\omega} R_{\mathrm{prt}} j_n(kR_{\mathrm{prt}}) Y_n^1(\theta,\phi) \sin\theta, \tag{13}$$

in which the latter integral returns simply to multiplication by 2π because the circumferentially symmetric harmonics Y_n^1 behave as constants in the integration.

The spatial integral of the *b*-field is calculated by integrating equation (13) along the Cartesian *z*-coordinate and turning the resulting integral back to spherical coordinates by the transformation $z = R_{\mathrm{prt}} \cos\theta$ and $\mathrm{d}z = -R_{\mathrm{prt}} \sin\theta \mathrm{d}\theta$ to exploit equation (9). We denote the unit vectors in *x* and *y* directions as $\hat{x}$ and $\hat{y}$. We get:

$$
\begin{aligned}
b_{\mathrm{prt}}^{\mathrm{eff}} |B_{R_{\mathrm{prt}}}| &= \int_{B_{R_{\mathrm{prt}}}} b(\hat{x}, \hat{y}) \mathrm{d}x \wedge \mathrm{d}y \wedge \mathrm{d}z \\
&= \int_{z=-R_{\mathrm{prt}}}^{R_{\mathrm{prt}}} \left(\int_{\partial S_z} a \right) \mathrm{d}z \\
&= \sum_{n=1}^{\infty} \frac{\alpha_n}{i\omega} R_{\mathrm{prt}} j_n(kR_{\mathrm{prt}}) 2\pi \int_{z=-R_{\mathrm{prt}}}^{R_{\mathrm{prt}}} Y_n^1(\theta, \phi) \sin\theta \mathrm{d}z \\
&= \sum_{n=1}^{\infty} \frac{\alpha_n}{i\omega} R_{\mathrm{prt}}^2 j_n(kR_{\mathrm{prt}}) 2\pi \int_{\theta=0}^{\pi} Y_n^1(\theta, \phi)(-\sin\theta) \sin\theta \mathrm{d}\theta \\
&= \sum_{n=1}^{\infty} 2\sqrt{\frac{2\pi}{3}} R_{\mathrm{prt}}^2 \frac{\alpha_n}{i\omega} j_n(kR_{\mathrm{prt}}) 2\pi \int_{\theta=0}^{\pi} Y_n^1(\theta, \phi) \frac{1}{2} \sqrt{\frac{3}{2\pi}} (-\sin\theta) \sin\theta \mathrm{d}\theta \\
&= \sum_{n=1}^{\infty} 2\sqrt{\frac{2\pi}{3}} \frac{\alpha_n}{i\omega} R_{\mathrm{prt}}^2 j_n(kR_{\mathrm{prt}}) \int_{\partial B_{R_{\mathrm{prt}}}} Y_n^1(\theta, \phi) Y_1^{1*}(\theta, \phi) \sin\theta \mathrm{d}\theta \wedge \mathrm{d}\phi \\
&= 2\sqrt{\frac{2\pi}{3}} \frac{\alpha_1}{i\omega} R_{\mathrm{prt}}^2 j_1(kR_{\mathrm{prt}}),
\end{aligned}
\tag{14}
$$

from which:

$$
b_{\mathrm{prt}}^{\mathrm{eff}} = \frac{2\sqrt{\frac{2\pi}{3}} \frac{\alpha_1}{i\omega} R_{\mathrm{prt}}^2 j_1(kR_{\mathrm{prt}})}{4/3\pi R_{\mathrm{prt}}^3} = \sqrt{\frac{3}{2\pi}} \frac{\alpha_1}{i\omega R_{\mathrm{prt}}} j_1(kR_{\mathrm{prt}}) \tag{15}
$$

follows.

This type of homogenization filters out the first mode of the magnetic flux density. If the boundary conditions of the particle are such that they excite other magnetic modes as well, their contribution is not visible in the homogenized flux density, but it would have to be lumped into the homogenized magnetic field strength. Furthermore, the first line of equation (14) shows that the spatial average is calculated against a vector frame. A Cartesian frame is chosen because we want the homogenized fields to be expressed in Cartesian coordinates. This choice of frame essentially defines an affine connection, thereby introducing an additional mathematical structure.

2.3 Effective energy-consistent modes

The particle experiences both magnetization and eddy currents. Our goal is to express the behavior of the particle in terms of a dynamic relationship between the homogenized quantities $b_{\mathrm{prt}}^{\mathrm{eff}}$ and $h_{\mathrm{prt}}^{\mathrm{eff}}$.

In the literature, energy balance is a key factor to be considered in homogenization (Corcolle *et al.*, 2021). Complex Poynting's theorem for peak-valued fields states:

$$-\frac{1}{2}\int_{\partial\Omega} e\wedge h^{*} = \frac{1}{2}\int_{\Omega} e\wedge j^{*} + \frac{i\omega}{2}\int_{\Omega} b\wedge h^{*} - \frac{i\omega}{2}\int_{\Omega} e\wedge d^{*}, \tag{16}$$

where the leftmost term represents the (complex) power flux through the boundary. In the absence of displacement currents, the last term vanishes, and only the first two terms on the right-hand side contribute to the energy exchange through the boundary. If the excitation is assumed to act only in the Cartesian z-direction, the left-hand side power is equated with $\frac{i\omega}{2} b_{\text{prt}}^{\text{eff}} h_{\text{prt}}^{\text{eff}} |\Omega|$, where $b_{\text{prt}}^{\text{eff}}$ and $h_{\text{prt}}^{\text{eff}}$ are the scalar components of homogenized fields. The quantity $h_{\text{prt}}^{\text{eff}}$ can be solved from the energy balance.

Let us consider the Poynting flux through the boundary surface, $\partial B_{R_{\text{prt}}}$ of the particle. For simplicity, we drop coefficient $\frac{1}{2}$ from equation (16) because it appears on both sides of the equation. Substituting the electric field (8) and tangential component of the magnetic field (12) into the Poynting flux term, we obtain:

$$\begin{aligned}
&-\int_{\partial B_{R_{\text{prt}}}} e\wedge h^{*} \\
&= -\sum_{n,m=1}^{\infty}\int_{\partial B_{R_{\text{prt}}}} \alpha_n R_{\text{prt}} j_n(kR_{\text{prt}}) Y_n^1(\theta,\phi) sin\theta \mathrm{d}\phi \wedge \left(\tfrac{\alpha_m}{i\omega\mu}\right)^{*} (j_m(kR_{\text{prt}}) + kR_{\text{prt}} j_m^{'}(kR_{\text{prt}}))^{*} Y_m^{1\,*}(\theta,\phi)\mathrm{d}\theta \\
&= \sum_{n,m=1}^{\infty} \alpha_n R_{\text{prt}} j_n(kR_{\text{prt}}) \left(\tfrac{\alpha_m}{i\omega\mu}\right)^{*} (j_m(kR_{\text{prt}}) + kR_{\text{prt}} j_m^{'}(kR_{\text{prt}}))^{*} \int_{\partial B_{R_{\text{prt}}}} Y_n^1(\theta,\phi) Y_m^{1\,*}(\theta,\phi) sin\theta \mathrm{d}\theta\wedge\mathrm{d}\phi \\
&= i\omega \sum_{n,m=1}^{\infty} \frac{\alpha_n}{i\omega} R_{\text{prt}} j_n(kR_{\text{prt}}) \left(\tfrac{\alpha_m}{i\omega\mu}\right)^{*} (j_m(kR_{\text{prt}}) + kR_{\text{prt}} j_m^{'}(kR_{\text{prt}}))^{*} \delta_{nm} \frac{3}{4\pi R_{\text{prt}}^3}\frac{4}{3}\pi R_{\text{prt}}^3 \\
&= i\omega \sum_{n,m=1}^{\infty} \underbrace{\sqrt{\frac{3}{2\pi}}\frac{\alpha_n}{i\omega R_{\text{prt}}} j_n(kR_{\text{prt}})}_{b_{\text{prt},n}^{\text{eff}}} \underbrace{\frac{1}{2}\sqrt{\frac{3}{2\pi}}\left(\frac{\alpha_m}{i\omega\mu R_{\text{prt}}}\right)^{*} (j_m(kR_{\text{prt}}) + kR_{\text{prt}} j_m^{'}(kR_{\text{prt}}))^{*}}_{h_{\text{prt},m}^{\text{eff}\,*}} \delta_{nm} |B_{R_{\text{prt}}}|. \\
&= i\omega \sum_{n=1}^{\infty} b_{\text{prt},n}^{\text{eff}} h_{\text{prt},n}^{\text{eff}\,*} |B_{R_{\text{prt}}}|
\end{aligned} \tag{17}$$

The interpretation is that all the energy exchanges are lumped into the effective scalar modes of h and b, given by $h_{\text{prt},n}^{\text{eff}}$ and $b_{\text{prt},n}^{\text{eff}}$. The modes are orthogonal in terms of Poynting flux. Family of reluctivities:

$$\nu_{\text{prt},n}^{\text{eff}} = \frac{h_{\text{prt},n}^{\text{eff}}}{b_{\text{prt},n}^{\text{eff}}} = \frac{j_n(kR_{\text{prt}}) + kR_{\text{prt}} j_n^{'}(kR_{\text{prt}})}{2\mu j_n(kR_{\text{prt}})} \tag{18}$$

is defined for $n = 1, 2, \ldots$. If all the magnetic modes are excited, all the reluctivities $\nu_{\text{prt},n}^{\text{eff}}$ with $n = 1, 2, \ldots$ participate in the energy exchange through the boundary of the particle. At this stage, the definitions of $h_{\text{prt},n}^{\text{eff}}$ and $b_{\text{prt},n}^{\text{eff}}$ in equation (17) need not be unique if considering only energy exchange. In fact, it suffices that the products $b_{\text{prt},n}^{\text{eff}} h_{\text{prt},n}^{\text{eff}\,*}$ coincide with what is stated in equation (17). Hence, the definitions of $\nu_{\text{prt},n}^{\text{eff}}$ for $n = 1, 2, \ldots$ are not unique. However, we already have good reasons to define them as in equations (17) and (18). First, in Subsection 2.2, we found a formula for $b_{\text{prt}}^{\text{eff}}$, that is equal to $b_{\text{prt},1}^{\text{eff}}$. Second, defining the rest of

the effective modes as in equation (17), the reluctivity modes in equation (18) all have a formula of the same form, differing only by the index n.

We are not fully statisfied with the formulas for $h^{\text{eff}}_{\text{prt},n}$ and $b^{\text{eff}}_{\text{prt},n}$ given in equation (17), because they contain unknown parameters α_n that are determined by the boundary conditions. Let us consider the tangential boundary conditions of h. The general form of the boundary values is:

$$h^{\text{tan}}_{\text{prt}} = -\sum_{n=1}^{\infty} \frac{\alpha_n}{i\omega\mu}\Big(j_n(kR_{\text{prt}}) + kR_{\text{prt}} j_n'(kR_{\text{prt}})\Big) Y^1_n(\theta, \phi)\mathrm{d}\theta. \tag{19}$$

Taking the inner product (9) of the boundary values, we get:

$$\begin{aligned}\langle h^{\text{tan}}_{\text{prt}}, Y^1_m \mathrm{d}\theta\rangle &= -\sum_{n=1}^{\infty} \frac{\alpha_n}{i\omega\mu}\big(j_n(kR_{\text{prt}}) + kR_{\text{prt}} j_n'(kR_{\text{prt}})\big)\langle Y^1_n \mathrm{d}\theta, Y^1_m \mathrm{d}\theta\rangle \\ &= -\frac{\alpha_m}{i\omega\mu}\Big(j_m(kR_{\text{prt}}) + kR_{\text{prt}} j_m'(kR_{\text{prt}})\Big).\end{aligned} \tag{20}$$

Substituting equation (20) into the definition of $h^{\text{eff}}_{\text{prt},m}$ in equation (17), $h^{\text{eff}}_{\text{prt},m}$ is simplified to:

$$h^{\text{eff}}_{\text{prt},m} = -\frac{1}{2}\sqrt{\frac{3}{2\pi}}\frac{1}{R_{\text{prt}}}\langle h^{\text{tan}}_{\text{prt}}, Y^1_m \mathrm{d}\theta\rangle, \tag{21}$$

which is completely determined by the boundary values and particle radius. Equation (21) provides the effective modes $h^{\text{eff}}_{\text{prt},n}$ for $n = 1, 2, \ldots$ a physical meaning. Obtaining such a simple physical meaning is another reason to define $h^{\text{eff}}_{\text{prt},n}$ and $b^{\text{eff}}_{\text{prt},n}$ as in equation (17). In a straightforward manner, we obtain:

$$b^{\text{eff}}_{\text{prt},n} = \frac{1}{\nu^{\text{eff}}_{\text{prt},n}} h^{\text{eff}}_{\text{prt},n} = -\sqrt{\frac{3}{2\pi}}\frac{\mu}{R_{\text{prt}}}\frac{j_n(kR_{\text{prt}})}{j_n(kR_{\text{prt}}) + kR_{\text{prt}} j_n'(kR_{\text{prt}})}\langle h^{\text{tan}}_{\text{prt}}, Y^1_n \mathrm{d}\theta\rangle, \tag{22}$$

which is determined by the boundary conditions. We conclude that the effective modes $h^{\text{eff}}_{\text{prt},n}$ in equation (21) and $b^{\text{eff}}_{\text{prt},n}$ in equation (22) can be calculated from the boundary conditions. These effective modes fully determine the power exchange through the boundary of the particle.

2.4 Homogenization of the magnetic field strength

Based on equations (15) and (17), we can state that $b^{\text{eff}}_{\text{prt}} = b^{\text{eff}}_{\text{prt},1}$. Regardless of the magnetic modes that are excited, homogenization only filters out the first effective mode of the b-field. If only the first magnetic mode is excited, homogenization becomes trivial. The reluctivity of the entire system is $\nu^{\text{eff}}_{\text{prt},1}$. This special case corresponds to the uniform magnetic excitation used in literature (Sato and Igarashi 2017). If other modes are also excited, their contribution to the total energy exchange must be lumped into $h^{\text{eff}}_{\text{prt}}$. Equating equation (17) with the homogenized power $i\omega b^{\text{eff}}_{\text{prt}} h^{\text{eff}*}_{\text{prt}} |B_{R_{\text{prt}}}|$, we obtain:

$$i\omega b_{\mathrm{prt}}^{\mathrm{eff}} h_{\mathrm{prt}}^{\mathrm{eff}\,*} |B_{R_{\mathrm{prt}}}| = i\omega \sum_{n=1}^{\infty} b_{\mathrm{prt},n}^{\mathrm{eff}} h_{\mathrm{prt},n}^{\mathrm{eff}\ *} |B_{R_{\mathrm{prt}}}|, \tag{23}$$

from which the homogenized magnetic field strength:

$$h_{\mathrm{prt}}^{\mathrm{eff}} = \sum_{n=1}^{\infty} \left(\frac{b_{\mathrm{prt},n}^{\mathrm{eff}}}{b_{\mathrm{prt}}^{\mathrm{eff}}} \right)^{*} h_{\mathrm{prt},n}^{\mathrm{eff}} = \sum_{n=1}^{\infty} \left(\frac{b_{\mathrm{prt},n}^{\mathrm{eff}}}{b_{\mathrm{prt},1}^{\mathrm{eff}}} \right)^{*} h_{\mathrm{prt},n}^{\mathrm{eff}} \tag{24}$$

can be solved. Substituting $h_{\mathrm{prt},n}^{\mathrm{eff}} = \nu_{\mathrm{prt},n}^{\mathrm{eff}} b_{\mathrm{prt},n}^{\mathrm{eff}}$ and equation (21), the effective reluctivity of the particle is given by:

$$\begin{aligned}
\nu_{\mathrm{prt}}^{\mathrm{eff}} &= \frac{h_{\mathrm{prt}}^{\mathrm{eff}}}{b_{\mathrm{prt}}^{\mathrm{eff}}} \\
&= \sum_{n=1}^{\infty} \left(\frac{b_{\mathrm{prt},n}^{\mathrm{eff}}}{b_{\mathrm{prt},1}^{\mathrm{eff}}} \right)^{*} \frac{h_{\mathrm{prt},n}^{\mathrm{eff}}}{b_{\mathrm{prt},1}^{\mathrm{eff}}} \\
&= \sum_{n=1}^{\infty} \left(\frac{\nu_{\mathrm{prt},1}^{\mathrm{eff}} h_{\mathrm{prt},n}^{\mathrm{eff}}}{\nu_{\mathrm{prt},n}^{\mathrm{eff}} h_{\mathrm{prt},1}^{\mathrm{eff}}} \right)^{*} \frac{h_{\mathrm{prt},n}^{\mathrm{eff}}}{h_{\mathrm{prt},1}^{\mathrm{eff}}} \nu_{\mathrm{prt},1}^{\mathrm{eff}} \\
&= \sum_{n=1}^{\infty} \frac{|\nu_{\mathrm{prt},1}^{\mathrm{eff}}|^2}{\nu_{\mathrm{prt},n}^{\mathrm{eff}\ *}} \frac{|h_{\mathrm{prt},n}^{\mathrm{eff}}|^2}{|h_{\mathrm{prt},1}^{\mathrm{eff}}|^2} \\
&= \sum_{n=1}^{\infty} \frac{|\nu_{\mathrm{prt},1}^{\mathrm{eff}}|^2}{\nu_{\mathrm{prt},n}^{\mathrm{eff}\ *}} \frac{|\langle h_{\mathrm{prt}}^{\tan},\, Y_n^1 \mathrm{d}\theta \rangle|^2}{|\langle h_{\mathrm{prt}}^{\tan},\, Y_1^1 \mathrm{d}\theta \rangle|^2},
\end{aligned} \tag{25}$$

which is fully determined by the boundary conditions $h_{\mathrm{prt}}^{\tan}$ of the h-field and the effective reluctivities $\nu_{\mathrm{prt},n}^{\mathrm{eff}}$ given in equation (18). This reluctivity is the main result of the first half of this paper. The second half of this study is dedicated to extending equation (25) to include the contribution of the insulating region around the particle.

3. Particle and insulation

In addition to the magnetic particle, we provide a treatment for the insulation region around it. The system is illustrated in Figure 1(b). The structure of this section is the same as the structure of Section 2.

3.1 Field solutions

Assuming that the insulation carries permeability μ_{ins} and the conductivity vanishes, the governing equation for the insulation is:

$$\star^{-1} \mathrm{d} \star^{-1} \mathrm{d} e = 0, \tag{26}$$

which is of Laplace type. For a circumferential electric field $e = e_{\phi} \mathrm{d}\phi$, equation (26) can be solved as:

$$e = -\sum_{n=1}^{\infty}\left(C_n r^{n+1} + D_n r^{-n}\right) Y_n^1(\theta, \phi)\sin\theta \mathrm{d}\phi, \tag{27}$$

where C_n and D_n are coefficients to be determined from the boundary conditions on the outer boundary of the insulation and the interface conditions on the boundary between the particle and insulation. Solutions (8) and (27) differ only by the radial function. We write the magnetic vector potential as $a = -\frac{1}{i\omega}e$, which yields:

$$a = \frac{1}{i\omega}\sum_{n=1}^{\infty}\left(C_n r^{n+1} + D_n r^{-n}\right) Y_n^1(\theta, \phi)\sin\theta \mathrm{d}\phi, \tag{28}$$

from which we calculate:

$$b = \sum_{n=1}^{\infty}\frac{1}{i\omega}\left[-\frac{\partial}{\partial r}\left(C_n r^{n+1} + D_n r^{-n}\right) Y_n^1(\theta, \phi)\sin\theta \mathrm{d}\phi\wedge\mathrm{d}r + \underbrace{\left(C_n r^{n+1} + D_n r^{-n}\right)\frac{\partial}{\partial\theta}\left(Y_n^1(\theta, \phi)\sin\theta\right)}_{\text{normal component}}\mathrm{d}\theta\wedge\mathrm{d}\phi\right], \tag{29}$$

$$h = \sum_{n=1}^{\infty}\frac{1}{i\omega\mu}\left[\underbrace{-\left((n+1)C_n r^n - nD_n r^{-n-1}\right) Y_n^1(\theta, \phi)}_{\text{tangential component}}\mathrm{d}\theta + \left(C_n r^n + D_n r^{-n-1}\right)\frac{\partial}{\partial\theta}\left(Y_n^1(\theta, \phi)\sin\theta\right)\frac{1}{r\sin\theta}\mathrm{d}r\right]. \tag{30}$$

Let us express the coefficients C_n and D_n in terms of α_n by equating the tangential components of h in equations (12) and (30) and the normal components of b in equations (11) and (29) at the interface between the particle and insulation, where $r = R_{\mathrm{prt}}$. We get two equations:

$$\alpha_n R_{\mathrm{prt}} j_n(kR_{\mathrm{prt}}) = C_n R_{\mathrm{prt}}^{n+1} + D_n R_{\mathrm{prt}}^{-n-1}, \tag{31}$$

and:

$$\frac{\alpha_n}{\mu}\left(j_n(kR_{\mathrm{prt}}) + kR_{\mathrm{prt}} j_n'(kR_{\mathrm{prt}})\right) = \frac{1}{\mu_{\mathrm{ins}}}\left((n+1)C_n R_{\mathrm{prt}}^n - nD_n R_{\mathrm{prt}}^{-n-1}\right), \tag{32}$$

from which we solve:

$$C_n = \underbrace{\alpha_n\left(\frac{2\mu_{\mathrm{ins}}\nu_{\mathrm{prt},n}^{\mathrm{eff}} + n}{2n+1}\right)}_{\beta_n} j_n(kR_{\mathrm{prt}}) R_{\mathrm{prt}}^{-n}, \tag{33}$$

and:

$$D_n = \underbrace{\alpha_n\left(\frac{(n+1) - 2\mu_{\mathrm{ins}}\nu_{\mathrm{prt},n}^{\mathrm{eff}}}{2n+1}\right)}_{\gamma_n} j_n(kR_{\mathrm{prt}}) R_{\mathrm{prt}}^{n+1}. \tag{34}$$

Substituting C_n and D_n into equations (27), (29) and (30), we obtain:

$$e = -\sum_{n=1}^{\infty} \alpha_n \left(\beta_n \left(\frac{r}{R_{\text{prt}}} \right)^{n+1} + \gamma_n \left(\frac{R_{\text{prt}}}{r} \right)^{n} \right) R_{\text{prt}} j_n(kR_{\text{prt}}) Y_n^1(\theta, \phi) \sin\theta \mathrm{d}\phi, \tag{35}$$

$$a = \sum_{n=1}^{\infty} \frac{\alpha_n}{i\omega} \left(\beta_n \left(\frac{r}{R_{\text{prt}}} \right)^{n+1} + \gamma_n \left(\frac{R_{\text{prt}}}{r} \right)^{n} \right) R_{\text{prt}} j_n(kR_{\text{prt}}) Y_n^1(\theta, \phi) \sin\theta \mathrm{d}\phi, \tag{36}$$

$$b = \sum_{n=1}^{\infty} \frac{\alpha_n}{i\omega} \Bigg[-\frac{\partial}{\partial r} \left(\beta_n \left(\frac{r}{R_{\text{prt}}} \right)^{n+1} + \gamma_n \left(\frac{R_{\text{prt}}}{r} \right)^{n} \right) R_{\text{prt}} j_n(kR_{\text{prt}}) Y_n^1(\theta, \phi) \sin\theta \mathrm{d}\phi \wedge \mathrm{d}r$$

$$\underbrace{+ \left(\beta_n \left(\frac{r}{R_{\text{prt}}} \right)^{n+1} + \gamma_n \left(\frac{R_{\text{prt}}}{r} \right)^{n} \right) R_{\text{prt}} j_n(kR_{\text{prt}}) \frac{\partial}{\partial\theta} \left(Y_n^1(\theta, \phi) \sin\theta \right) \mathrm{d}\theta \wedge \mathrm{d}\phi}_{\text{normal component}} \Bigg], \tag{37}$$

$$h = \sum_{n=1}^{\infty} \frac{\alpha_n}{i\omega\mu} \Bigg[\underbrace{-\left((n+1)\beta_n \left(\frac{r}{R_{\text{prt}}} \right)^{n} - n\gamma_n \left(\frac{R_{\text{prt}}}{r} \right)^{n+1} \right) j_n(kR_{\text{prt}}) Y_n^1(\theta, \phi)}_{\text{tangential component}} \mathrm{d}\theta$$

$$+ \left(\beta_n \left(\frac{r}{R_{\text{prt}}} \right)^{n} + \gamma_n \left(\frac{R_{\text{prt}}}{r} \right)^{n+1} \right) j_n(kR_{\text{prt}}) \frac{\partial}{\partial\theta} \left(Y_n^1(\theta, \phi) \sin\theta \right) \frac{1}{r\sin\theta} \mathrm{d}r \Bigg], \tag{38}$$

that are valid in the insulation, where $R_{\text{prt}} < r < R_{\text{ins}}$.

3.2 Homogenization of the magnetic flux density

The calculation of the homogenized magnetic flux density follows the treatment described in Section 2.2. Instead of repeating the same calculations starting from the a-field (36), we can exploit solution (15). We first observe that the restriction of the a-field (36) to the outer boundary of the insulation, where $r = R_{\text{ins}}$, is:

$$a(R_{\text{ins}}, \theta, \phi) = \sum_{n=1}^{\infty} \underbrace{\left(\beta_n \left(\frac{R_{\text{ins}}}{R_{\text{prt}}} \right)^{n+1} + \gamma_n \left(\frac{R_{\text{prt}}}{R_{\text{ins}}} \right)^{n} \right)}_{\kappa_n} \frac{\alpha_n}{i\omega} R_{\text{prt}} j_n(kR_{\text{prt}}) Y_n^1(\theta, \phi) \sin\theta \mathrm{d}\phi, \tag{39}$$

where the coefficients κ_n are the only difference between equations (39) and (10). Hence, the calculations are very similar to those in Section 2.2, and we show only the necessary manipulations. Following the treatment given in equation (14), we obtain:

$$b_{\text{ins}}^{\text{eff}}|B_{R_{\text{ins}}}| = \int_{B_{R_{\text{ins}}}} b(\hat{x},\hat{y})\mathrm{d}x\wedge\mathrm{d}y\wedge\mathrm{d}z$$
$$= \sum_{n=1}^{\infty}\kappa_n\frac{\alpha_n}{i\omega}R_{\text{prt}}j_n(kR_{\text{prt}})2\pi\int_{z=-R_{\text{ins}}}^{R_{\text{ins}}} Y_n^1(\theta,\phi)\sin\theta\mathrm{d}z$$
$$= \sum_{n=1}^{\infty}\kappa_n 2\sqrt{\frac{2\pi}{3}}\frac{\alpha_n}{i\omega}R_{\text{ins}}R_{\text{prt}}j_n(kR_{\text{prt}})\delta_{n,1}$$
$$= \kappa_1 2\sqrt{\frac{2\pi}{3}}\frac{\alpha_1}{i\omega}R_{\text{ins}}R_{\text{prt}}j_1(kR_{\text{prt}}). \quad (40)$$

The only differences between equations (14) and (40) are that in equation (40), the coefficient κ_1 appears, and the integration is associated with the radius R_{ins} instead of R_{prt}. From equation (40), it follows that:

$$b_{\text{ins}}^{\text{eff}} = \frac{\kappa_1 2\sqrt{\frac{2\pi}{3}}\frac{\alpha_1}{i\omega}R_{\text{ins}}R_{\text{prt}}j_1(kR_{\text{prt}})}{4/3\pi R_{\text{ins}}^3}$$
$$= \sqrt{\frac{3}{2\pi}}\frac{\alpha_1}{i\omega R_{\text{ins}}}\left(\beta_1\left(\frac{R_{\text{ins}}}{R_{\text{prt}}}\right)+\gamma_1\left(\frac{R_{\text{prt}}}{R_{\text{ins}}}\right)^2\right)j_1(kR_{\text{prt}}). \quad (41)$$

3.3 Effective energy-consistent modes

Substituting the tangential parts of the *e*- and *h*-fields, equations (35) and (38), to the Poynting flux integral, we obtain:

$$-\int_{\partial B_{R_{\text{ins}}}} e\wedge h^* = \sum_{n,m=1}^{\infty}\alpha_n\left(\beta_n\left(\frac{R_{\text{ins}}}{R_{\text{prt}}}\right)^{n+1}+\gamma_n\left(\frac{R_{\text{prt}}}{R_{\text{ins}}}\right)^n\right)R_{\text{prt}}j_n(kR_{\text{prt}})$$
$$\left(\frac{\alpha_m}{i\omega\mu}\right)^*\left((m+1)\beta_m\left(\frac{R_{\text{ins}}}{R_{\text{prt}}}\right)^m - m\gamma_m\left(\frac{R_{\text{prt}}}{R_{\text{ins}}}\right)^{m+1}\right)^*$$
$$j_m^*(kR_{\text{prt}})\int_{\partial B_{R_{\text{ins}}}} Y_n^1(\theta,\phi)Y_m^{1*}(\theta,\phi)sin\theta\mathrm{d}\theta\wedge\mathrm{d}\phi$$
$$= i\omega\sum_{n,m=1}^{\infty}\frac{\alpha_n}{i\omega}\left(\beta_n\left(\frac{R_{\text{ins}}}{R_{\text{prt}}}\right)^{n+1}+\gamma_n\left(\frac{R_{\text{prt}}}{R_{\text{ins}}}\right)^n\right)R_{\text{prt}}j_n(kR_{\text{prt}})$$
$$\left(\frac{\alpha_m}{i\omega\mu}\right)^*\left((m+1)\beta_m\left(\frac{R_{\text{ins}}}{R_{\text{prt}}}\right)^m - m\gamma_m\left(\frac{R_{\text{prt}}}{R_{\text{ins}}}\right)^{m+1}\right)^* j_m^*(kR_{\text{prt}})\delta_{nm}\frac{3}{4\pi R_{\text{ins}}^3}\frac{4}{3}\pi R_{\text{ins}}^3$$

$$= i\omega \sum_{n,m=1}^{\infty} \underbrace{\sqrt{\frac{3}{2\pi}} \frac{\alpha_n}{i\omega R_{\text{ins}}} \left(\beta_n \left(\frac{R_{\text{ins}}}{R_{\text{prt}}} \right)^n + \gamma_n \left(\frac{R_{\text{prt}}}{R_{\text{ins}}} \right)^{n+1} \right) j_n(kR_{\text{prt}})}_{b_{\text{ins},n}^{\text{eff}}}$$

$$\underbrace{\frac{1}{2} \sqrt{\frac{3}{2\pi}} \left(\frac{\alpha_m}{i\omega\mu R_{\text{ins}}} \right)^* \left((m+1)\beta_m \left(\frac{R_{\text{ins}}}{R_{\text{prt}}} \right)^m - m\gamma_m \left(\frac{R_{\text{prt}}}{R_{\text{ins}}} \right)^{m+1} \right)^* j_m^*(kR_{\text{prt}})}_{h_{\text{ins},m}^{\text{eff}\,*}} \delta_{nm} |B_{R_{\text{ins}}}|.$$

$$= i\omega \sum_{n=1}^{\infty} b_{\text{ins},n}^{\text{eff}} h_{\text{ins},n}^{\text{eff}\,*} |B_{R_{\text{ins}}}| \tag{42}$$

We note that the homogenized $b_{\text{ins}}^{\text{eff}}$ coincides with $b_{\text{ins},1}^{\text{eff}}$. Furthermore, the modes are orthogonal in terms of Poynting flux. Family of reluctivities:

$$\nu_{\text{ins},n}^{\text{eff}} = \frac{(n+1)\beta_n \left(\frac{R_{\text{ins}}}{R_{\text{prt}}} \right)^n - n\gamma_n \left(\frac{R_{\text{prt}}}{R_{\text{ins}}} \right)^{n+1}}{2\mu_{\text{ins}} \left[\beta_n \left(\frac{R_{\text{ins}}}{R_{\text{prt}}} \right)^n + \gamma_n \left(\frac{R_{\text{prt}}}{R_{\text{ins}}} \right)^{n+1} \right]} \tag{43}$$

is defined based on the orthogonality of the modes.

We want to express the effective modes $h_{\text{ins},n}^{\text{eff}}$ and $b_{\text{ins},n}^{\text{eff}}$ in terms of the boundary conditions. The general form of the boundary conditions for h at the outer boundary of the insulation is:

$$h_{\text{ins}}^{\tan} = -\sum_{n=1}^{\infty} \frac{\alpha_n}{i\omega\mu} \left((n+1)\beta_n \left(\frac{R_{\text{ins}}}{R_{\text{prt}}} \right)^n - n\gamma_n \left(\frac{R_{\text{prt}}}{R_{\text{ins}}} \right)^{n+1} \right) j_n(kR_{\text{prt}}) Y_n^1(\theta, \phi) \mathrm{d}\theta. \tag{44}$$

Taking the inner product (9) from the boundary conditions, we get:

$$\begin{aligned} \langle h_{\text{ins}}^{\tan}, Y_m^1 \mathrm{d}\theta \rangle &= -\sum_{n=1}^{\infty} \frac{\alpha_n}{i\omega\mu} \left((n+1)\beta_n \left(\frac{R_{\text{ins}}}{R_{\text{prt}}} \right)^n - n\gamma_n \left(\frac{R_{\text{prt}}}{R_{\text{ins}}} \right)^{n+1} \right) j_n(kR_{\text{prt}}) \langle Y_n^1 \mathrm{d}\theta, Y_m^1 \mathrm{d}\theta \rangle \\ &= -\frac{\alpha_m}{i\omega\mu} \left((m+1)\beta_m \left(\frac{R_{\text{ins}}}{R_{\text{prt}}} \right)^m - m\gamma_m \left(\frac{R_{\text{prt}}}{R_{\text{ins}}} \right)^{m+1} \right) j_m(kR_{\text{prt}}). \end{aligned} \tag{45}$$

Substituting the inner product to the definition (42) of $h_{\text{ins},n}^{\text{eff}}$, we get:

$$h_{\text{ins},m}^{\text{eff}} = -\frac{1}{2} \sqrt{\frac{3}{2\pi}} \frac{1}{R_{\text{ins}}} \langle h_{\text{ins}}^{\tan}, Y_m^1 \mathrm{d}\theta \rangle, \tag{46}$$

which is very much of the same form as equation (21), except that the radius R_{prt} is replaced by R_{ins}. Furthermore:

$$b^{\text{eff}}_{\text{ins},n} = \frac{1}{\nu^{\text{eff}}_{\text{ins},n}} h^{\text{eff}}_{\text{ins},n} = -\sqrt{\frac{3}{2\pi}} \frac{\mu_{\text{ins}}}{R_{\text{ins}}} \frac{\beta_n \left(\frac{R_{\text{ins}}}{R_{\text{prt}}}\right)^n + \gamma_n \left(\frac{R_{\text{prt}}}{R_{\text{ins}}}\right)^{n+1}}{(n+1)\beta_n \left(\frac{R_{\text{ins}}}{R_{\text{prt}}}\right)^n - n\gamma_n \left(\frac{R_{\text{prt}}}{R_{\text{ins}}}\right)^{n+1}} \langle h^{\tan}_{\text{ins}}, Y^1_m \mathrm{d}\theta \rangle. \tag{47}$$

Using equations (46) and (47), the losses can be directly calculated from the boundary values.

3.4 Homogenization of the magnetic field strength

For the particle/insulation system, we found that homogenization filtered out only the first mode of the *b*-field. Hence, the energy contributions of the remaining modes must be lumped into the homogenized *h*-field.

First, we notice that the representation of losses in equation (23) in terms of the effective modes is the same for the particle/insulation -system (replacing subscripts prt with ins) as for a bare particle due to the modes being orthogonal. Second, the coefficients before the inner products in the effective modes in equation (46) do not depend on the mode indices. It follows from these two observations that Section 2.4 applies directly to the particle/insulation system just by changing the subscripts prt, referring to a bare particle, to ins, referring to a particle/insulation system. The homogenized reluctivity of the system is given by:

$$\nu^{\text{eff}}_{\text{ins}} = \sum_{n=1}^{\infty} \frac{|\nu^{\text{eff}}_{\text{ins},1}|^2}{\nu^{\text{eff}\ *}_{\text{ins},n}} \frac{|\langle h^{\tan}_{\text{ins}}, Y^1_n \mathrm{d}\theta \rangle|^2}{|\langle h^{\tan}_{\text{ins}}, Y^1_1 \mathrm{d}\theta \rangle|^2}, \tag{48}$$

where $\nu^{\text{eff}}_{\text{ins},n}$ are the mode-reluctivities, given in equation (43), $h^{\tan}_{\text{ins}}$ are the tangential boundary values of the *h*-field on the outer boundary of the insulation and Y^1_n are the scalar spherical harmonic functions whose normalization is defined in equation (9). To use the formula, it is necessary to substitute the symbols $\nu^{\text{eff}}_{\text{ins},n}$, β_n, γ_n and $\nu^{\text{eff}}_{\text{prt},n}$. These can be found in equations (43), (33), (34), and (18). Equation (48) is the main contribution of this study.

4. Numerical examples

The validity of the derived methods is demonstrated in the mathematical treatment of this study. A numerical treatment is presented in this section. To further argue that there is no mistake in the formulas or their practical implementations, a finite element model is provided for comparison.

The physics of the problem is encapsulated in the system (2)−(6). For the numerical formulation, the so-called "$T-\Omega$" formulation is used. The magnetic field strength h is expressed as $h = t - \mathrm{d}\lambda$, where t is a current vector potential and λ is a magnetic scalar potential. The scalar potential λ is defined everywhere, whereas t is defined only within the conductive particle. The tangential trace of t is set to zero on the boundary of the particle, ensuring that the current density does not penetrate this boundary surface. The scalar potential is assigned boundary conditions on the outer surface of the entire domain, which in turn control the tangential boundary conditions of the magnetic field strength.

In the conductive domain, we set:

$$\mathrm{d}\left((\star\sigma)^{-1}\mathrm{d}t\right) = -j\omega\left(\star\mu(t - \mathrm{d}\lambda)\right), \tag{49}$$

$$\mathrm{d}\left(\star\mu(t-\mathrm{d}\lambda)\right)=0, \tag{50}$$

where μ and σ are the permeability and conductivity of the particle, respectively. In the insulation, we set:

$$\mathrm{d}(\star\mu_{\mathrm{ins}}\mathrm{d}\lambda)=0, \tag{51}$$

where μ_{ins} is the permeability of the insulation.

Homogenization of the fields from the finite element solutions is performed based on the same principles as those in the analytical treatment. The flux density is homogenized by averaging, and the field strength is homogenized by evaluating the following energy-based formula:

$$h_{\mathrm{FEM}}^{\mathrm{eff}}:=\left(\frac{2p}{i\omega b_{\mathrm{FEM}}^{\mathrm{eff}}}\right)^{*}, \tag{52}$$

where $h_{\mathrm{FEM}}^{\mathrm{eff}}$ is the homogenized field strength, $b_{\mathrm{FEM}}^{\mathrm{eff}}$ is the homogenized flux density and p is the average complex power density. This defines $h_{\mathrm{FEM}}^{\mathrm{eff}}$ using the complex power formula $p=\frac{1}{2}i\omega b_{\mathrm{FEM}}^{\mathrm{eff}}h_{\mathrm{FEM}}^{\mathrm{eff}\ *}$, where the homogenized quantities are peak-valued.

The permeability of the particle $\mu=1000\mu_0$ and the insulation $\mu_{\mathrm{ins}}=\mu_0$ are selected. Conductivity of the particle is set to $\sigma=10^7$ S/m. For "virtual insulation" in Figures 3(a) and 3(b), the radii $R_{\mathrm{prt}}=R_{\mathrm{ins}}=$ 10 μm. The term virtual insulation means that actual insulation is not considered, yet the current density is prevented from penetrating the boundary of the particle. Figures 3(a) and 3(b) include an additional axis a/δ, where $a=2R_{\mathrm{prt}}$ is a characteristic length of the particle and δ is the skin depth. For "insulation" in Figures 3(c)

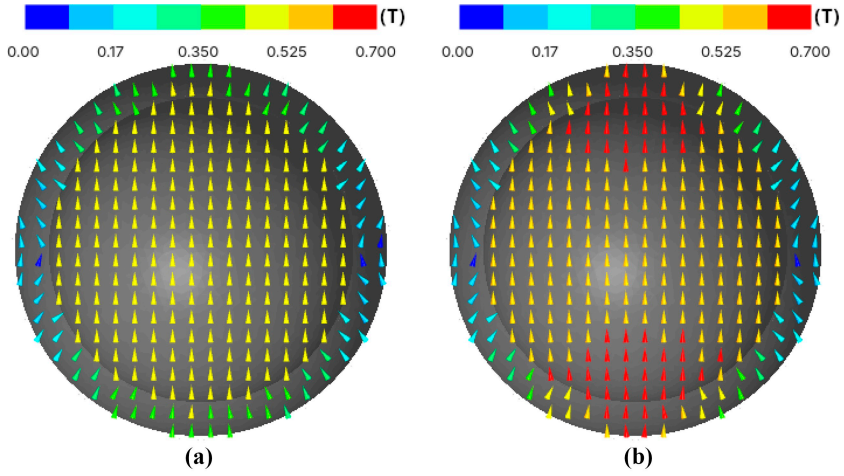

Figure 2. Real part of the magnetic flux density from 1-Hz finite element simulations; (a) Uniform excitation, (b) Polar-focused excitation

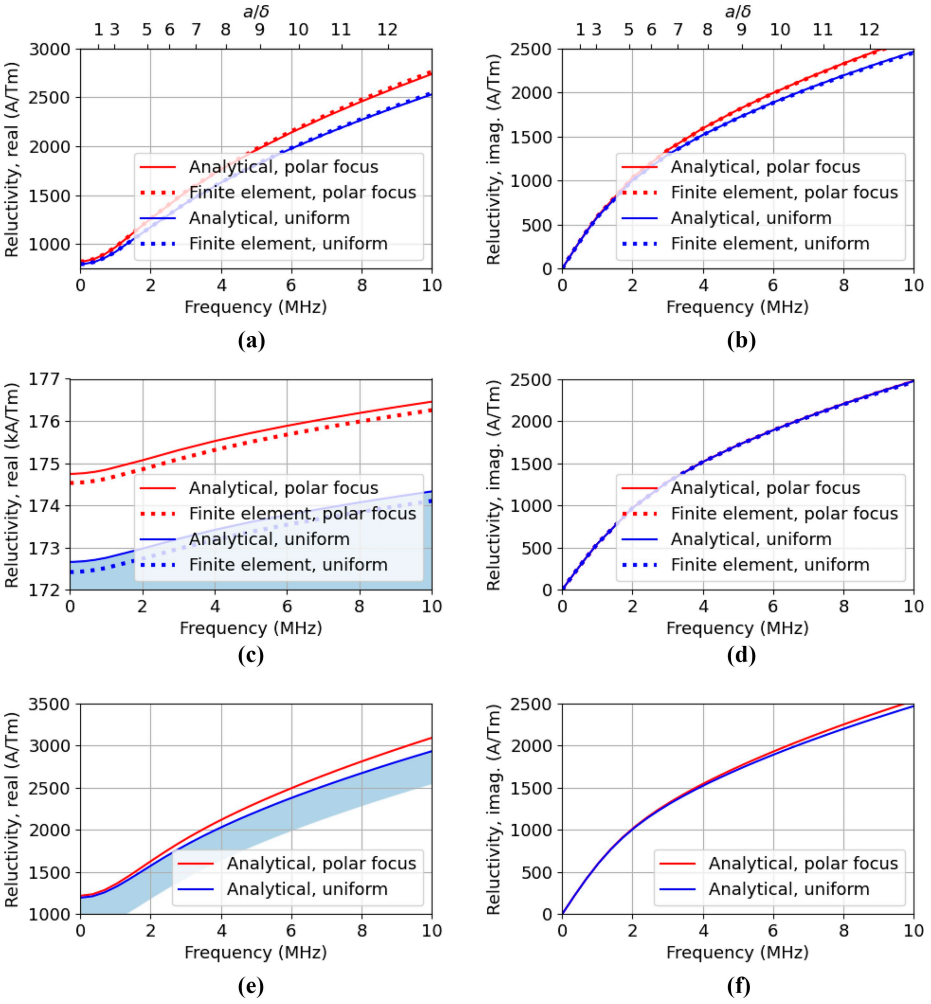

Figure 3. Homogenized reluctivities. Comparison between (48) and numerical solutions, (a) Virtual insulation, real reluctivity, (b) Virtual insulation, imaginary reluctivity, (c) 2 μm insulation, real reluctivity with Hashin−Shtrikman bounds, (d) 2 μm insulation, imaginary reluctivity, (e) 5 nm insulation, real reluctivity with Hashin−Shtrikman bounds, (f) 5 nm insulation, imaginary reluctivity

and 3(d), $R_{\text{prt}} = 9\,\mu\text{m}$ and $R_{\text{ins}} = 11\,\mu\text{m}$. In Figures 3(a)-3(f), the "uniform" boundary conditions are $h_{\text{ins}}^{\tan} = -10^3 \sin\theta \mathrm{d}\theta$, and the boundary conditions with "polar focus" are $h_{\text{ins}}^{\tan} = -10^3 \mathrm{d}\theta$. Figures 3(e) and 3(f), contain calculations with substantially thinner insulations. In these cases, the insulations are 5 nm thick. Figures 3(a), 3(c) and 3(e) also include the Hashin−Shtrikman bounds for the homogenized reluctivity (Hashin and Shtrikman 1962). They are defined as:

$$\nu_{\mathrm{HS1}} = \left(\Re\{\nu_{\mathrm{prt}}^{\mathrm{eff}}\}^{-1} + \frac{1 - \left(\frac{R_{\mathrm{prt}}}{R_{\mathrm{ins}}}\right)^3}{\frac{1}{\mu_{\mathrm{ins}} - \Re\{\nu_{\mathrm{prt}}^{\mathrm{eff}}\}^{-1}} + \frac{\left(\frac{R_{\mathrm{prt}}}{R_{\mathrm{ins}}}\right)^3}{3\Re\{\nu_{\mathrm{prt}}^{\mathrm{eff}}\}^{-1}}} \right)^{-1}, \tag{53}$$

$$\nu_{\mathrm{HS2}} = \left(\mu_{\mathrm{ins}} + \frac{\left(\frac{R_{\mathrm{prt}}}{R_{\mathrm{ins}}}\right)^3}{\frac{1}{\Re\{\nu_{\mathrm{prt}}^{\mathrm{eff}}\}^{-1} - \mu_{\mathrm{ins}}} + \frac{1 - \left(\frac{R_{\mathrm{prt}}}{R_{\mathrm{ins}}}\right)^3}{3\mu_{\mathrm{ins}}}} \right)^{-1}. \tag{54}$$

The effective particle reluctivity $\nu_{\mathrm{prt}}^{\mathrm{eff}}$ is used together with the "uniform" boundary conditions, because this is one of the assumptions underlying the Hashin−Shtrikman bounds. In the case of the virtually insulated particle in Figure 3(a), both bounds coincide with the "uniform" curves.

Low-frequency visualizations of the magnetic flux density can be found in Figure 2. These visualizations reveal the differences in the selected boundary conditions. Figures 3(a)−3(d) show that the numerical calculations agree with the results obtained by equation (48). This gives further evidence that the mathematical treatment in this study is correct. Figures 3(a) and 3(b) also show that model (48) is effective when some higher order magnetic modes are excited by the boundary conditions. Figures 3(c) and 3(d) show that adding insulation around the particle renders the imaginary parts of the homogenized reluctivities independent of the two chosen boundary conditions. This indicates that the effect of higher-order modes on the losses of the system tends to decay when more insulation is added around the particle. In Figure 3(c), the analytical and finite-element results differ to some extent. This is because the solutions are dominated by the insulation, and discretization errors within the insulation become visible in the real parts of the responses. As the mesh is refined, the curves converge toward those obtained from the analytical formulas. It would be difficult to obtain the results shown in Figures 3(e) and 3(f) using the finite element method, since the insulation would require an extremely dense mesh. In contrast, evaluating the analytical formulas is straightforward, illustrating one of the advantages of analytical methods over finite element computations. The reluctivities computed using the "uniform" boundary conditions in Figures 3(a), 3(c) and 3(e) fall within the Hashin–Shtrikman bounds. The reluctivities computed using the "polar-focus" boundary conditions lie outside these bounds, because the bounds cannot account for more complex boundary conditions.

The magnetoquasistatic model is valid throughout the investigated frequency range. This can be verified by comparing the particle diameter with the wavelength $\lambda = \left(f\sqrt{\varepsilon_0\mu}\right)^{-1}$, where f is the frequency, ε_0 is the vacuum permittivity and μ is the particle permeability. For $f = 10$ MHz and $\mu = 1000\mu_0$, the resulting wavelength is $\lambda = 95$ cm, which is approximately 10^5 times larger than the particle diameter. We therefore conclude that wave-propagation effects can be neglected.

5. Conclusion

This paper proposes a formula for the homogenized reluctivity of an insulated magnetic particle with nonzero conductivity. The model admits arbitrary but circumferentially symmetric boundary conditions for the magnetic field strength in the polar direction. The novelty is condensed in equation (48). With the proposed model, it is possible to consider the effects of the insulation and boundary conditions of particles more flexibly. The presented

mathematical treatment together with numerical examples provide validation for the proposed model.

Some new perspectives have been provided for homogenization. The relationships between energy-consistent effective magnetic modes, boundary conditions and homogenizations were investigated. The first effective mode of the magnetic flux density coincided with the spatial average of the flux density. It was discussed that homogenization through spatial averaging of the flux density involves a special structure, since such averaging involves a 2-form-valued integral. Hence, a vector frame was chosen against which the components of the flux density were extracted and averaged. Such a choice essentially defines an affine connection, which introduces an additional mathematical structure. The Cartesian vector frame was chosen for this purpose because material models tend to be identified in the Cartesian frame. The effects of the other magnetic modes were combined into the homogenized field strength in terms of energy balance.

For the investigated systems, it was possible to homogenize the flux density and field strength at the boundary of the system. It is sufficient to know the tangential parts of the electric field strength, magnetic field strength and magnetic vector potential on the boundary of the system to obtain the homogenized fields.

References

Abramowitz, M., and Stegun, I.A. (1965), "Handbook of Mathematical Functions: with Formulas, Graphs, and Mathematical Tables", 9th Revised edition Dover Publications, New York, NY:

Advanced Electromagnetic Field Analysis for Effective Design (2016), "Tech. rep. 1391", pp. 21-40.

Bordianu, A. *et al.* (2012), "A multiscale approach to predict classical losses in soft magnetic composites", In *IEEE Transactions on Magnetics*, Vol. 48 No. 4, pp. 1537-1540.

Bossavit, A. (1995), "On the homogenization of Maxwell equations", *COMPEL - The International Journal for Computation and Mathematics in Electrical and Electronic Engineering*, Vol. 14 No. 4, pp. 23-26.

Bottauscio, O., Chiampi, M. and Manzin, A. (2009), p. (3946), "Homogenized magnetic properties of heterogeneous anisotropic structures including nonlinear media", *IEEE Transactions on Magnetics*, Vol. 45 No. 10, p. 3949.

Bottauscio, O. *et al.* (2006), "Electromagnetic phenomena in heterogeneous media: effective properties and local behavior", *Journal of Applied Physics*, Vol. 100 No. 4, p. 044902.

Corcolle, R., Ren, X. and Daniel, L. (2021), "Effective properties and eddy current losses of soft magnetic composites", *Journal of Applied Physics*, Vol. 129 No. 1, p. 015103.

Gyselinck, J. and Vandevelde, L. *et al.* (1999), "Calculation of eddy currents and associated losses in electrical steel laminations", *IEEE Transactions on Magnetics 35.3. Conference Name: IEEE Transactions on Magnetics*, pp. 1191-1194.

Gyselinck, J., Sabariego, R.V. and Dular, P. (2006), "A nonlinear time-domain homogenization technique for laminated iron cores in three-dimensional finite-element models", *IEEE Transactions on Magnetics*, Vol. 42 No. 4, pp. 763-766.

Hashin, Z. and Shtrikman, S. (1962), "A variational approach to the theory of the effective magnetic permeability of multiphase materials", *Journal of Applied Physics*, Vol. 33 No. 10, pp. 3125-3131.

Ito, Y. and Igarashi, H. (2013), "Computation of macroscopic electromagnetic properties of soft magnetic composite", *IEEE Transactions on Magnetics*, Vol. 49 No. 5, pp. 1953-1956.

Kameari, A. (2015), "Eddy current analysis using polynomial functions in curvilinear orthogonal coordinate systems", In: *The Papers of Joint Technical Meeting on "Static Apparatus" and "Rotating Machinery"*, IEE Japan, Tosa, Japan, pp. 45-50.

Lindell, I.V. (2004), "Differential forms in electromagnetics", *IEEE Press Series on Electromagnetic Wave Theory*, IEEE Press [u.a.], Piscataway, NJ.

Maruo, A. and Igarashi, H. (2019), "Analysis of magnetic properties of soft magnetic composite using discrete element method", *IEEE Transactions on Magnetics*, Vol. 55 No. 6, pp. 1-5.

Ren, X., Corcolle, R. and Daniel, L. (2016), "Losses approximation for soft magnetic composites based on a homogenized equivalent conductivity", *Advanced Electromagnetics*, Vol. 5 No. 2, p. 59.

Ren, X., Corcolle, R. and Daniel, L. (2016), "A homogenization technique to calculate eddy current losses in soft magnetic composites using a complex magnetic permeability", *IEEE Transactions on Magnetics*, Vol. 52 No. 12, pp. 1-9.

Sato, H. and Igarashi, H. (2021), "3-D analysis of soft magnetic composite using discrete element method in frequency domain", *IEEE Transactions on Magnetics*, Vol. 57 No. 6, pp. 1-4.

Sato, H., Kotani, J., Sasaki, Y., Tomioka, S., Takizawa, T., Ueda, Y., Kimiya, H. and Igarashi, H. (2024), "Analysis of magnetic properties of soft magnetic composite using magnetic circuits generated by discrete element method", *IEEE Transactions on Magnetics*, Vol. 60 No. 12, pp. 1-7.

Sato, T. *et al*. (2015), "Loss computation of soft magnetic composite inductors based on interpolated scalar magnetic property", *IEEE Transactions on Magnetics*, Vol. 51 No. 3, pp. 1-4.

Sato, Y. and Igarashi, H. (2016), "Time-domain analysis of soft magnetic composite using equivalent circuit obtained via homogenization", In: *2016 IEEE Conference on Electromagnetic Field Computation (CEFC). Miami, FL*: *IEEE*, p. 1.

Sato, Y. and Igarashi, H. (2017), "Time-domain analysis of soft magnetic composite using equivalent circuit obtained via homogenization". In", *IEEE Transactions on Magnetics*, Vol. 53, pp. 1-4.

Shokrollahi, H. and Janghorban, K. (2007), "Soft magnetic composite materials (SMCs)", *Journal of Materials Processing Technology*, Vol. 189 Nos 1-3, pp. 1-12.

Corresponding author
Joonas Vesa can be contacted at: joonas.vesa@tuni.fi

COMPEL - The international journal for computation and mathematics in electrical and electronic engineering